Check for updates

Synthesis of a cubane-like anion [Re4As2S2(CN)12]6− for coordinate regulation of Na+ ion transport†

Hongyang Li, [ID] [a,b] Andrey V. Ermolaev, [ID] [b] Aleksei S. Pronin,[b] Jingang Zheng,[a] Hao Huang,[a] Han Zhang, [ID] [a] Lixiang Li, [ID] [a] Baigang An, [ID] *[a] Yuri V. Mironov [ID] *[b] and Chengguo Sun [ID] *[a,c]

A cyanometallate cluster compound Na6[Re4As2S2(CN)12] (NRASCN) as a Na+ ionic conductor, has been synthesized by a simple solid-state synthetic route. The X-ray structural analysis shows that the structure contains a typical rhenium tetrahedron that is surrounded by the mixed ligands of μ3-As and μ3-S to form cubane-like cluster cores. The Na+ ions are well-distributed around cyanide groups and form a disordered sublattice spanning three and four Na crystallographic sites. The Na+ ionic conductor NRASCN exhibits a high ionic conductivity of 1.05×10^{-5} S cm^{-1} at 25 °C. Using the PEO−NaTFSI−NRASCN composite electrolyte, an all-solid-state battery with a Na metal anode and a NaVPO4 (NVP) cathode, shows a high specific capacity (109.4 mA h g^{-1}) and stable long-term cycling performance (1000 cycles) at a rate of 0.3 C.

Introduction

Transition metal cluster complexes (TMCCs) that consist of metal frameworks connected by metal-to-metal bonds have developed rapidly due to their unique physical and chemical properties suitable for catalysts, magnetic materials, photodynamic therapy and X-ray contrast agents.[1–6] Among them, so-called "high-valence clusters" are typically formed by d-metals of groups 5–7 with chalcogenide inner ligands.[7] For example, the cubane-like cluster core of Re4Q4 (Q = S, Se, Te) is the main component of these typical complexes.[8] The [Re4Q4(CN)12]4− cluster core is commonly used in the synthesis of coordination polymers with d-metal and f-metal ions. It is worth mentioning that this cluster core possesses a rigid geometry due to the two interpenetrating Re4 and Q4 tetrahedra, and the bidentate terminal cyano (CN) groups.[9,10]

Generally, the properties of cluster compounds strongly depend on the ligands attached to the metal atoms.[11] For M4Q4 cluster cores (M = Mo, W, Re, and Q = S, Se, Te), the chalcogenide ions S2−, Se2−, and Te2− commonly serve as inner-sphere μ3-ligands.[12,13] However, our research group has recently found that both CCN3− and As3− ligands are capable of acting as inner-sphere μ3-ligands.[14] The CCN3− ligands were synthesized by CN− oxidation with W6+ reduction in organometallic compounds. As3− also can, instead of CCN3−, bridge the triangles of W atoms in high temperature reactions. Other works have also demonstrated that the mixed-ligand tetrahedral rhenium complex Re4As6S3 can be synthesized by heating the elements in sealed evacuated quartz tubes.[15] Considering the cubane-like structure and the diversity of ligand-dependence, we conceived the idea of M4Q4 cluster cores with CN− ligands for coordinate regulation of Na+ ion transport, thus obtaining a stable Na+ ionic conductor material.

As we all know, Na+ ionic conductors are crucial factors to realize high-performance all-solid-state Na-ion batteries (Na-ASSBs). Typical Na+ ionic conductors can be divided into three categories including oxide-based ionic conductors (β-Al2O3, NASICON), sulfide-based ionic conductors (Na3PS4, Na10SnP2S12), and hydride-based ionic conductors (NaBH4, Na3AlH6).[16–18] The complexes of M4Q4 cluster cores have barely been explored as Na+ ionic conductors. It is speculated that structural properties, such as the construction of metal-to-metal bonds, and introduction of the appropriate ligand might be the major reasons for restriction of the coordination and transfer of Na+ ions in an M4Q4 skeleton.

Adjusting the outer ligands of an M4Q4 skeleton is an efficient way to improve cationic coordination and physico-

[a] Key Laboratory of Energy Materials and Electrochemistry Liaoning Province, School of Chemical Engineering, University of Science and Technology Liaoning, Anshan 114051, China

[b] Nikolaev Institute of Inorganic Chemistry, Siberian Branch of the Russian Academy of Sciences, Novosibirsk 630090, Russia. E-mail: yuri@niic.nsc.ru

[c] School of Chemical Engineering, Nanjing University of Science and Technology, Nanjing, Jiangsu 210094, China

†Electronic supplementary information (ESI) available. CCDC 2329960. For ESI and crystallographic data in CIF or other electronic format see DOI: https://doi.org/10.1039/d4qi01151a

This journal is © the Partner Organisations 2024

Inorg. Chem. Front., 2024, **11**, 6671–6678 | **6671**

chemical properties. Herein, we synthesized a novel rhenium cluster complex $Na_6[Re_4As_2S_2(CN)_{12}]\cdot0.75CH_3OH\cdot6H_2O$ containing mixed ligands in its core. X-ray structural analysis was performed to determine the structural integrity. After removing the solvents (CH_3OH and H_2O molecules) and pressing it into an electrolyte pallet, NRASCN exhibits acceptable ionic conductivity (1.05×10^{-5} S cm^{-1} at 25 °C), which is comparable to that of the known $Na_3Zr_2Si_2PO_{12}$-based solid-state electrolyte at 30 °C (1.53×10^{-5} S cm^{-1}),[19] and better than that of Na_3AlH_6 (5×10^{-7} S cm^{-1}).[16] To further demonstrate its electrochemical performance and reduce the interface resistance in Na-ASSBs, we have prepared a composite electrolyte (PEO–NaTFSI–NRASCN) comprising a poly(ethylene oxide) (PEO) matrix, sodium bis(trifluoromethanesulfonyl)imide (NaTFSI) salts, and the Na$^+$ ionic conductor NRASCN. The Na|PEO–NaTFSI–NRASCN|NVP cells exhibit superior rate performance and good cycling stability for 1000 cycles. The finding provides an alternative way to prepare transition metal cluster Na$^+$ ionic conductors for high performance Na-ASSBs.

Experimental

Material synthesis

Single crystal $Na_6[Re_4As_2S_2(CN)_{12}]\cdot0.75CH_3OH\cdot6H_2O$ was synthesized by a simple solid-state synthetic route. ReI$_3$ was prepared by the reaction of HReO$_4$ with HI as described earlier.[20] A mixture of ReI$_3$ (0.53 mmol), sodium cyanide (3.18 mmol), and arsenic trisulfide (0.27 mmol) was thoroughly triturated in a mortar and sealed in an evacuated quartz tube. The tube was heated to 550 °C for 4 h, and kept at this temperature for 48 h, then cooled to 50 °C h^{-1}. The reaction products were dissolved in water, refluxed, and filtered off. The brown solution was concentrated to 3 mL and cooled to room temperature. The target product as brown crystals was isolated by the diffusion of CH_3OH vapor into the H_2O solution. The yield of $Na_6[Re_4As_2S_2(CN)_{12}]\cdot0.75CH_3OH\cdot6H_2O$ was 20%. The NRASCN polycrystalline powders were obtained by removing the solvents under vacuum at 200 °C for 24 h.

The PEO–NaTFSI–NRASCN composite electrolyte was prepared using a solution casting method. The raw materials PEO ($M_w = 1 \times 10^6$ g mol^{-1}) and NaTFSI should be dried under vacuum at 60 °C for 24 h before use. Both PEO (0.500 g) and NaTFSI (EO/Na = 16/1 in molar ratio) were dissolved in 20 mL of acetonitrile with moderate stirring, then NRASCN (10 wt%) was added to obtain a homogeneous solution. The mixture was continuously stirred at room temperature for 12 h, then was poured into a polytetrafluoroethylene mold, and dried in a vacuum oven at 60 °C for 24 h. Finally, the dry electrolyte was obtained and punched into small plates with a diameter of 19 mm.

The preparation of cathodes and cell assembly details are shown in the ESI.†

Characterization

A single crystal of the compound was selected directly from the reaction mixtures and glued to the tip of glass fibers using epoxy resin. The X-ray powder diffraction pattern (XRD) for the synthesized compound shows good agreement with that simulated from the crystal structure. According to the XRD patterns, the compound is phase pure and air-stable. Single-crystal X-ray diffraction data were collected using monochromatized Mo Kα radiation ($\lambda = 0.71073$ Å) on a Bruker D8 Venture diffractometer equipped with a Bruker PHOTON III area detector at 150 K. Absorption correction was applied empirically (over the intensities of equivalent reflections) using the SADABS program.[21] The crystal structure was solved by direct methods. The hydrogen atoms of water molecules were not located. Hydrogen atoms of –CH$_3$, and –OH groups of the MeOH molecule were set geometrically. The final refinement was performed using the full-matrix least-squares technique in the anisotropic approximation for all non-hydrogen atoms over independent reflections. All calculations were carried out using the SHELXL-2018/3 program package.[22] Figures were drawn using the DIAMOND program.[23]

All electrochemical measurements were carried out on an electrochemical station (Biologic VSP300). The AC impedance measurements were carried out on a workstation over the frequency range 3 MHz to 0.1 Hz with an amplitude of 10 mV. Before the AC impedance measurement, the cell was kept at the test temperature for 2 h to reach thermal equilibrium. The ionic conductivity σ_{ion} was calculated from the following equation:

$$\sigma_{ion} = \frac{d}{S \times R_b}$$

where d (cm) is the thickness of the solid-state electrolyte, S (cm^2) is the area of the electrode, and R_b (Ω) is the bulk resistance of the electrolyte measured by AC impedance measurement.[24] The ionic conductivity is temperature-dependent and typically shows Arrhenius behavior:
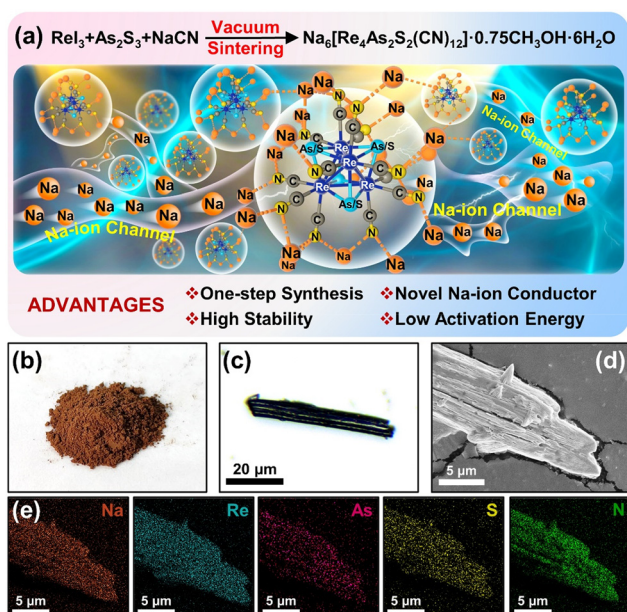
$$\sigma_{ion} = A \exp\left(-\frac{E_a}{RT}\right)$$

where E_a is the activation energy in kJ mol^{-1}, A is the pre-exponential factor, $R \approx 8.314$ J mol^{-1} K^{-1} is the ideal gas constant, and T (K) is the temperature.[24]

The LAND CT2001A (Wuhan Land Electronics Co. Ltd) test system was used to perform cell measurements. The charge–discharge voltage range was 2.5–3.9 V vs. Na/Na$^+$ for cathodes. The 1 C rate was determined and found to be 117 mA h g^{-1} in NVP cell testing.

The materials used and thermostability characterization details are shown in the ESI.†

Results and discussion

Over the last few years, our group has devoted itself to rhenium cluster complexes with mixed ligands using ReI$_3$ as a precursor.[25–28] Inspired by these interesting research studies, we continue to synthesize rhenium cluster complexes with group 15 elements, especially for arsenic and sulfur. Fig. 1a

6672 | *Inorg. Chem. Front.*, 2024, **11**, 6671–6678

This journal is © the Partner Organisations 2024

Fig. 1 (a) Schematic diagram for the preparation of crystal and Na-ion transport channels. (b) Digital photograph of $Na_6[Re_4As_2S_2(CN)_{12}]\cdot0.75CH_3OH\cdot6H_2O$ powder. (c) Optical photograph of $Na_6[Re_4As_2S_2(CN)_{12}]\cdot0.75CH_3OH\cdot6H_2O$ crystal. (d) SEM image of the crystal and (e) corresponding EDS mapping of Na, Re, As, S, and N elements.

shows the preparation of crystals using a simple vacuum sintering method and the schematic diagram of Na-ion transport channels. The reaction of ReI_3 and As_2S_3 with NaCN will result

in the formation of a brownish powder (digital photograph in Fig. 1b). After diffusion of CH_3OH vapor into the H_2O solution of NRASCN, the brown crystal of $Na_6[Re_4As_2S_2(CN)_{12}]\cdot0.75CH_3OH\cdot6H_2O$ was collected for X-ray structural analysis (optical photograph in Fig. 1c). The scanning electron microscopy (SEM) image (Fig. 1d) further confirms the polygonal morphology of the crystal, and the corresponding energy-dispersive X-ray spectroscopy (EDS) mapping (Fig. 1e) analysis reveals the presence of Na, Re, As, S, and N elements. The crystallographic data and refinement details are summarized in Table S1 (ESI†).

Fig. 2a shows a fragment of the crystal structure of the $Na_6[Re_4As_2S_2(CN)_{12}]\cdot0.75CH_3OH\cdot6H_2O$ cluster (CCDC 2329960†), and shows that it crystallizes in the triclinic $P\bar{1}$ space group. Every asymmetric unit contains 4 Re atoms, 4 mixed As/S atoms, 12 CN groups, and 7 Na positions (2 positions are half-occupied). However, the crystal is obtained by vapor diffusion of CH_3OH to H_2O; 0.75 solvate CH_3OH and 6 H_2O molecules are present in the crystal structure. In the case of the cluster anion, $[Re_4As_2S_2(CN)_{12}]^{6-}$ displays a slightly distorted geometry in comparison with the typical cubane-like cluster core containing 12 cluster valence electrons.[29] The Re–Re distances for the face coordinated by the sulfide ligand lie in the range from 2.775(4) to 2.794(4) Å with an average value of 2.786(8) Å. This is well consistent with the typical Re–Re bond lengths in $Cp_2Re_2B_6H_6$, indicating the similar electronegativities of $[B_6H_6]^{2-}$ and As^{3-} ligands.[30] The measured interval for Re–(As/S) bond lengths is 2.416(1) to 2.457(1) Å, which is somewhat longer than the Re–S bond lengths (2.346 Å) in the Re_4S_4 cluster core.[9] These values agree well with the
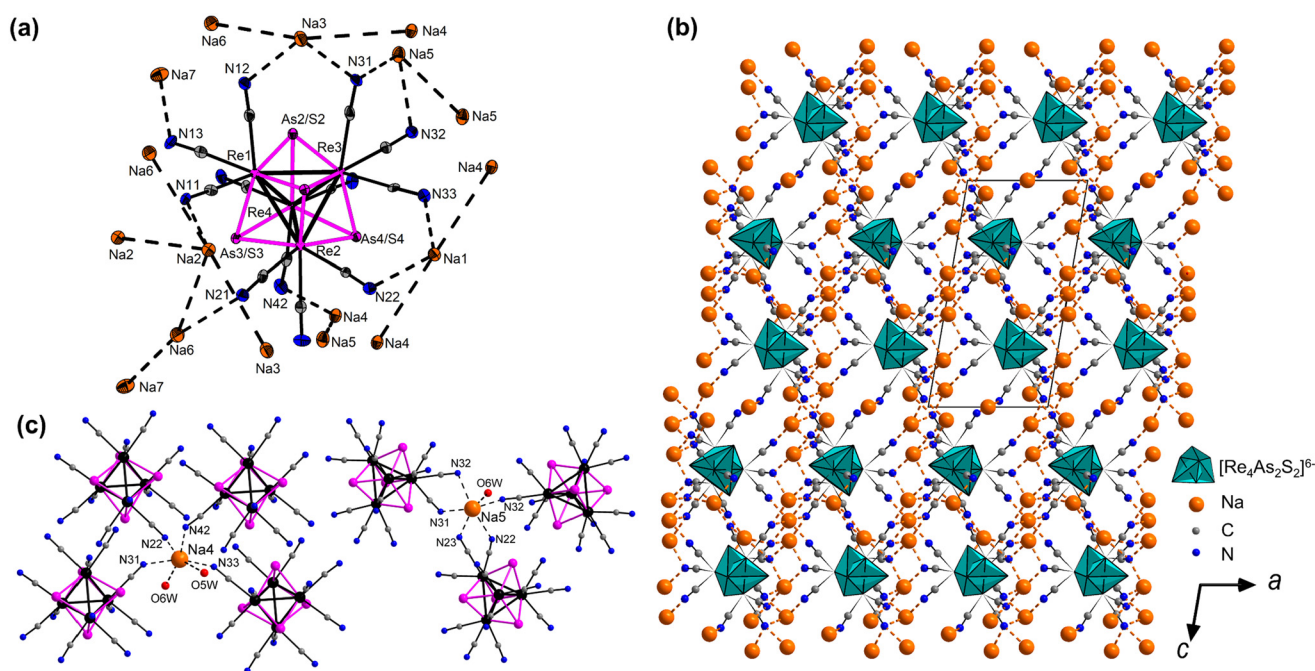
Fig. 2 (a) The fragment of crystal structure of $Na_6[Re_4As_2S_2(CN)_{12}]\cdot0.75CH_3OH\cdot6H_2O$. (b) The packing of the structure projected along the crystallographic axis *b*. (c) The two typical types of Na^+ ion coordination model.

This journal is © the Partner Organisations 2024

Inorg. Chem. Front., 2024, **11**, 6671–6678 | **6673**

Research Article

reported Re–(As/S) bond lengths in $[\{Re_6S_6As_2\}(PPr_3)_6]$, where As and S inner ligands share the same positions.[31] Each Re atom of the $\{Re_4As_2S_2\}^{6+}$ core is coordinated by three terminal CN^- ligands. The Re–C distances are in the typical range of 2.090(7)–2.132(8) Å (average 2.109(13) Å). The packing of the structure projected along the crystallographic axis b is shown in Fig. 2b. It consists of triclinic unit cells, a = 9.4363(3) Å, b = 10.2986(2) Å and c = 17.6142(4) Å. Great lattice parameters usually imply the presence of a large channel size for Na^+ ion migration to promote Na^+ ionic conductivity.[32] Meanwhile, the cell packing presents a layered structure, along the continuous long-range channels formed by the framework anions enriched with Na^+ ions, which promote Na^+ ion movement back and forth in the NRASCN. Fig. 2c shows the two typical types of Na^+ ion coordination, which occupy three and four crystallographically independent positions with the 4 and 5 nitrogen atoms in the arrangement of sodium and 2 or 1 oxygen atoms of coordinated water respectively. The coordination numbers of all sodium atoms equal 6. The coordination environment primarily involves nitrogen atoms of CN groups. The high dielectric CN groups benefit the higher degree of dissociation of ion salts, which can promote ion transport.[33]

To further investigate the crystalline phase, the $Na_6[Re_4As_2S_2(CN)_{12}]\cdot0.75CH_3OH\cdot6H_2O$ powder was studied by XRD in the 2θ angle range of 5–50°; it was found that the prepared $Na_6[Re_4As_2S_2(CN)_{12}]\cdot0.75CH_3OH\cdot6H_2O$ has obvious characteristic peaks at 9.14, 10.00, 10.39, 10.92 and 11.69° (Fig. 3a), indicating high crystallinity. In contrast, the simulated XRD pattern was also calculated from the structural parameters, which is almost the same as the experimental data. The results demonstrated the high phase purity of the $Na_6[Re_4As_2S_2(CN)_{12}]\cdot0.75CH_3OH\cdot6H_2O$ sample. Its thermal stability shows that the structure of $Na_6[Re_4As_2S_2(CN)_{12}]\cdot0.75CH_3OH\cdot6H_2O$ starts to break down above 700 °C (Fig. 3b). The weight loss below 100 °C corresponds to the removal of crystal methanol and water.
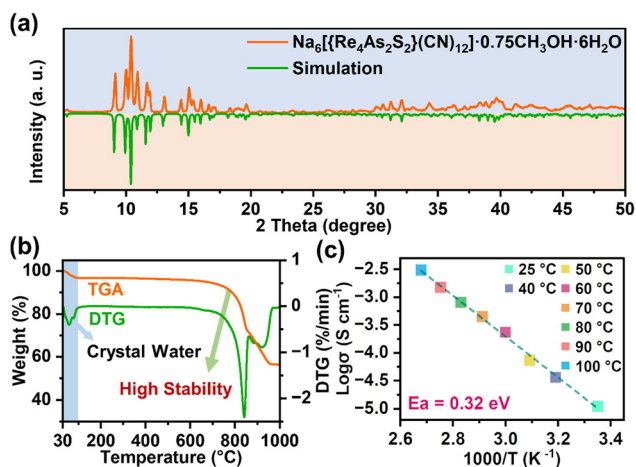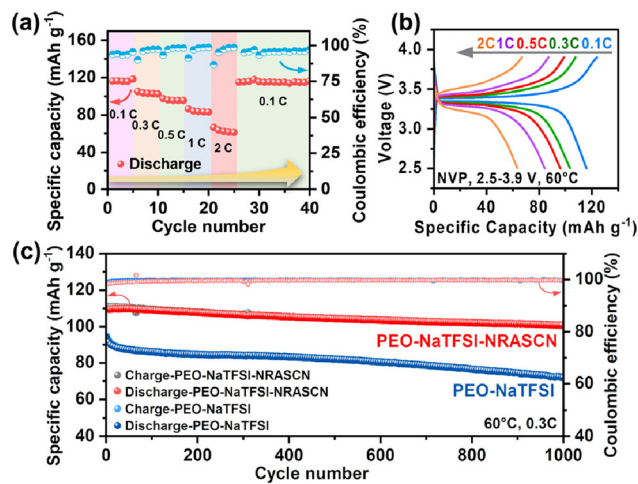
To avoid the corrosion of trace CH_3OH and H_2O on the electrodes, the $Na_6[Re_4As_2S_2(CN)_{12}]\cdot0.75CH_3OH\cdot6H_2O$ powders were treated at 200 °C for 24 h under vacuum to remove the crystal solvents.[34,35] It was found that the absorption peaks around 3500 cm^{-1} that were assigned to methanol and water disappeared (Fig. S1, ESI†), indicating that $Na_6[Re_4As_2S_2(CN)_{12}]\cdot0.75CH_3OH\cdot6H_2O$ converted to NRASCN. To gain a better insight into the Na^+ ion transport properties of NRASCN, the NRASCN tablet was obtained by cold pressing under a pressure of 300 MPa with a diameter of 12 mm and a thickness of 4 mm. Then, the blocking cells were assembled with a stainless steel electrode and an NRASCN tablet with both surfaces coated with Pt. The ionic conductivities of NRASCN were evaluated using the AC impedance measurements at a series of temperatures (25–100 °C) in order to get an Arrhenius plot. As the Nyquist plots of impedance shown in Fig. S2 (ESI†) indicate, NRASCN exhibits an acceptable Na^+ ionic conductivity of 1.05×10^{-5} S cm^{-1} at 25 °C, which is comparable to that of known $Na_3Zr_2Si_2PO_{12}$-based solid-state electrolytes at 30 °C (1.53×10^{-5} S cm^{-1}),[19] and better than that of Na_3AlH_6 (5×10^{-7} S cm^{-1}).[16] Based on the Arrhenius plot, the corresponding activation energy (Fig. 3c) was calculated at about 0.32 eV, smaller than that of $Na_{2.5}Zr_2Si_{1.5}P_{1.5}O_{12}$ (0.39 eV).[36] NRASCN exhibits a much higher ionic conductivity and lower activation energy than the previously reported electrodes in Table S2 (ESI†). The reason for this can be attributed to the CN^- ligand coordination and abundant Na^+ vacancies in NRASCN.[33,37,38] The larger CN group coordination induces longer Na–C bonds and decreases the Coulomb force between Na and N atoms. It is worth mentioning that the Na vacancies in NRASCN are produced by a loss of crystal solvent.[39] As shown in Fig. S3 and S4 (ESI†), NRASCN has a lower average formation energy (2.71 eV) than $Na_6[Re_4As_2S_2(CN)_{12}]\cdot0.75CH_3OH\cdot6H_2O$ (3.88 eV) according to DFT calculations, indicating that NRASCN is more likely to form abundant vacancies. Meanwhile, NRASCN shows an order of magnitude increase in ionic conductivity, owing to the Na^+ vacancies and CN^- ligand coordination (Fig. S5, ESI†).

Although the ionic conductivity of NRASCN meets the requirements of Na-ASSBs for ion transport at room temperature, the interface resistance is still a major bottleneck that restricts the performance of solid-state batteries.[40] As shown in Fig. S6 (ESI†), the NVP|NRASCN|Na cell shows a high interface impedance of around 3712 Ω, which can be attributed to the solid–solid interface contact between the electrodes and electrolyte. To further explore the function of NRASCN in Na-ASSBs, we have prepared a composite electrolyte (PEO–NaTFSI–NRASCN) comprising PEO matrix, NaTFSI salt, and an NRASCN conductor. The SEM images and corresponding EDS results (Fig. S7, ESI†) show a uniform distribution of NRASCN in PEO–NaTFSI–NRASCN, and the thickness is approximately 50 μm (Fig. S8, ESI†). In contrast to the PEO–NaTFSI electrolyte (9.60×10^{-6} S cm^{-1} at 25 °C), the PEO–NaTFSI–NRASCN composite electrolyte shows a superior ionic conductivity as high as 5.43×10^{-5} S cm^{-1} at 25 °C (Fig. S9, ESI†), the main reason

Fig. 3 (a) The XRD pattern and simulation of crystal structure of $Na_6[Re_4As_2S_2(CN)_{12}]\cdot0.75CH_3OH\cdot6H_2O$. (b) The TGA and DTG curves of $Na_6[Re_4As_2S_2(CN)_{12}]\cdot0.75CH_3OH\cdot6H_2O$. (c) Arrhenius plot of NRASCN.

6674 | *Inorg. Chem. Front.*, 2024, **11**, 6671–6678

This journal is © the Partner Organisations 2024

Fig. 4 Electrochemical performance of Na|PEO−NaTFSI−NRASCN|NVP Na-ASSBs at 60 °C. (a and b) Charge−discharge profiles and rate performance at various current densities of 0.1−2 C. (c) Long-term profile of Na|PEO−NaTFSI−NRASCN|NVP cell and Na|PEO−NaTFSI|NVP at 0.3 C.

Fig. 5 (a and b) High resolution XPS elemental composition analysis of Na surface. (c and d) SEM images of Na anode surface after 200 cycles at 0.3 C.

for this being the good ability of NRASCN to transport Na$^+$ ions and enhance the PEO chain segment motion.

Fig. 4a and b illustrate the charge/discharge capacities of the Na|PEO−NaTFSI−NRASCN|NVP cell at different C rates at 60 °C. The cell delivers an initial capacity of 116.1 mA h g^{-1} at 0.1 C, approaching 99.3% of the theoretical value. At 0.3 C, 0.5 C, 1 C and 2 C, the discharge capacities were approximately 104.9, 97.4, 86.4, and 66.4 mA h g^{-1}, respectively. Fig. 4c shows the long term cycling performance of both Na|PEO−NaTFSI−NRASCN|NVP and Na|PEO−NaTFSI|NVP cells at 0.3 C. After 1000 cycles, Na|PEO−NaTFSI−NRASCN|NVP cells maintain a capacity of 100.5 mA h g^{-1}. In contrast, the Na|PEO−NaTFSI|NVP cells only exhibit a low capacity of 72.0 mA h g^{-1}. Na|PEO−NaTFSI−NRASCN|NVP cells show a longer cycle life capacity and higher retention than the previously reported electrodes in Table S3 (ESI†).

To evaluate the compatibility between NRASCN and Na metal, the contact angle between NRASCN and molten Na was measured. Fig. S10 (ESI†) shows a satisfactory contact angle of 20°, indicating that NRASCN has good compatibility with Na. Fig. S11a and b (ESI†) show the evolution of the electrochemical impedance spectra for the Na|PEO−NaTFSI−NRASCN|Na and Na|PEO−NaTFSI|Na symmetric cells for different storage times. No significant changes of the impedance spectra were observed for Na|PEO−NaTFSI−NRASCN|Na, indicating that NRASCN possesses good compatibility and stability of the sodium metal. Fig. S12 (ESI†) shows the sodium plating/stripping test for Na|PEO−NaTFSI−NRASCN|Na and Na|PEO−NaTFSI|Na cells at a current density of 0.05 mA cm^{-2} and 60 °C. The Na|PEO−NaTFSI−NRASCN|Na cell was cycled for more than 200 h with a stable and lower overvoltage (112 mV). In contrast, the Na|PEO−NaTFSI|Na cell could only cycle for about 24 h along with an erratic voltage profile.
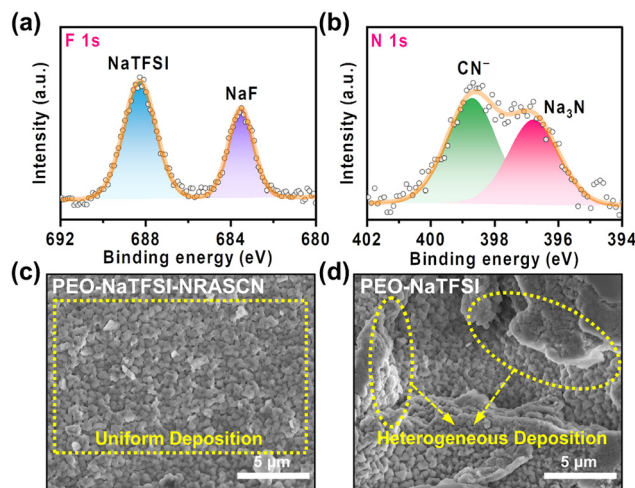
To identify the interface chemistry of the solid-state interface layer, X-ray photoelectron spectroscopy (XPS) measurements were carried out to confirm the surface composition of the Na anode. The Na|PEO−NaTFSI−NRASCN|NVP cells were allowed to undergo 200 charge/discharge cycles at 0.3 C. The Na anode was also carefully peeled off from the composite electrolyte. As shown in Fig. 5a and b, the high resolution F 1s and N 1s spectra show strong peaks. The inorganic components NaF (683.5 eV) and Na$_3$N (396.7 eV) at the interface layer[41,42] accelerate Na$^+$ ion transport and improve the performance and stability of the cells.[43,44] SEM was performed to visualize the surface morphology of the Na anode after Na plating/stripping for 200 cycles. As shown in Fig. 5c, compared to the heterogeneous deposition of Na with PEO−NaTFSI (Fig. 5d), uniform Na deposition on the surface of the PEO−NaTFSI−NRASCN electrolyte was obtained. It is worth noting that the Na anode paired with the PEO−NaTFSI−NRASCN electrolyte exhibits a smooth surface and uniform Na deposition at a higher magnification (Fig. S13a, ESI†). In contrast, a moss-like dendrite surface is observed when using the PEO−NaTFSI electrolyte (Fig. S13b, ESI†).

Conclusions

In summary, we synthesized a cyanometallate cluster compound Na$_6$[Re$_4$As$_2$S$_2$(CN)$_{12}$]·0.75CH$_3$OH·6H$_2$O. All the solvent molecules were removed after heating beyond 200 °C under vacuum. Based on the X-ray structural analysis, we discussed in detail the characteristic crystal structure and spatial arrangement of atoms. Combining this with electrochemical analysis, we confirmed that NRASCN has the ability to transport Na$^+$ ions, and exhibits an ionic conductivity of 1.05×10^{-5} S cm^{-1} at 25 °C. NRASCN used as a novel ionic conductor in the PEO−NaTFSI−NRASCN composite electrolyte can achieve a long

cycle life (1000 cycles at 0.3 C) and high capacity retention (91.8%). This work provides a design strategy for preparing Na^+ ionic conductor materials.

Author contributions

Hongyang Li: conceptualization, methodology, investigation, data curation, and writing the original draft. Andrey V. Ermolaev: investigation, data curation and writing – review and editing. Aleksei S. Pronin: methodology and data curation. Jingang Zheng: formal analysis and data curation. Hao Huang: formal analysis and data curation. Han Zhang: data curation and validation. Lixiang Li: writing – review and editing. Baigang An: conceptualization, funding acquisition and supervision. Yuri V. Mironov: conceptualization, project administration, and supervision. Chengguo Sun: writing – review and editing, funding acquisition, and supervision.

Data availability

The data that support the findings of this study are available from the corresponding author upon reasonable request. Crystallographic data have been deposited at the Cambridge Crystallographic Data Centre as a supplementary publication No. 2329960.

Conflicts of interest

There are no conflicts to declare.

Acknowledgements

References

1 F. A. Cotton, Discovering and understanding multiple metal-to-metal bonds, *Acc. Chem. Res.*, 1978, **11**, 225–232.

2 S. Chen, Y. Gao, W. Wang, O. V. Prezhdo and L. Xu, Prediction of three-metal cluster catalysts on two-dimensional W_2N_3 support with integrated descriptors for electrocatalytic nitrogen reduction, *ACS Nano*, 2023, **17**, 1522–1532.

3 F. Yang, P. Hu, F. F. Yang, B. Chen, F. Yin, R. Sun, K. Hao, F. Zhu, K. Wang and Z. Yin, Emerging enhancement and regulation strategies for ferromagnetic 2D transition metal dichalcogenides, *Adv. Sci.*, 2023, **10**, 2300952.

4 X.-Y. Wang, C. Avendaño and K. R. Dunbar, Molecular magnetic materials based on 4d and 5d transition metals, *Chem. Soc. Rev.*, 2011, **40**, 3213–3238.

5 K. Kirakci, M. A. Shestopalov and K. Lang, Recent developments on luminescent octahedral transition metal cluster complexes towards biological applications, *Coord. Chem. Rev.*, 2023, **481**, 215048.

6 A. A. Krasilnikova, A. O. Solovieva, A. A. Ivanov, K. E. Trifonova, T. N. Pozmogova, A. R. Tsygankova, A. I. Smolentsev, E. I. Kretov, D. S. Sergeevichev, M. A. Shestopalov, Y. V. Mironov, A. M. Shestopalov, A. F. Poveshchenko and L. V. Shestopalova, Comprehensive study of hexarhenium cluster complex $Na_4[\{Re_6Te_8\}(CN)_6]^-$ in terms of a new promising luminescent and X-ray contrast agent, *Nanomedicine*, 2017, **13**, 755–763.

7 J. Zhang, X. Bu, P. Feng and T. Wu, Metal chalcogenide supertetrahedral clusters: Synthetic control over assembly, dispersibility, and their functional applications, *Acc. Chem. Res.*, 2020, **53**, 2261–2272.

8 Y. V. Mironov, T. E. Albrecht-Schmitt and J. A. Ibers, Syntheses and characterizations of the new tetranuclear rhenium cluster compounds $Re_4(\mu_3\text{-}Q)_4(TeCl_2)_4Cl_8$ (Q = S, Se, Te), *Inorg. Chem.*, 1997, **36**, 944–946.

9 V. P. Fedin, M. R. J. Elsegood, W. Clegg and A. G. Sykes, High-yield synthesis of the cuboidal rhenium cluster $[Re_4S_4(CN)_{12}]^{4-}$ by reaction of the triangular cluster $[Re_3S_7Br_6]^+$ with cyanide, *Polyhedron*, 1996, **15**, 485–488.

10 Y. V. Mironov, N. G. Naumov, K. A. Brylev, O. A. Efremova, V. E. Fedorov and K. Hegetschweiler, Rhenium–chalcogenide–cyano clusters, Cu^{2+} ions, and 1,2,3,4-tetraaminobutane as molecular building blocks for chiral coordination polymers, *Angew. Chem., Int. Ed.*, 2004, **43**, 1297–1300.

11 K. Bhattacharjee and B. L. V. Prasad, Surface functionalization of inorganic nanoparticles with ligands: A necessary step for their utility, *Chem. Soc. Rev.*, 2023, **52**, 2573–2595.

12 R. Hernández-Molina and A. G. Sykes, Chalcogenide-bridged cuboidal clusters with M_4Q_4 (M = Mo, W; Q = S, Se, Te) cores, *J. Chem. Soc., Dalton Trans.*, 1999, **18**, 3137–3148.

13 Y. V. Mironov and V. E. Fedorov, Tetranuclear rhenium chalcogenide cluster complexes with a cubane core. Synthesis, structures, and properties, *Russ. Chem. Bull.*, 2002, **51**, 569–580.

14 S. S. Yarovoy, A. I. Smolentsev, S. G. Kozlova, N. B. Kompankov, Y. M. Gayfulin, I. P. Asanov, V. V. Yanshole and Y. V. Mironov, From oxide to a new type of molecular tungsten compound: Formation of bitetrahedral cluster complexes $[\{W_6(\mu_4\text{-}O)_2(\mu_3\text{-}CCN)_4\}(CN)_{16}]^{10-}$ and $[\{W_6(\mu_4\text{-}O)_2(\mu_3\text{-}As)_4\}(CN)_{16}]^{10-}$, *Chem. Commun.*, 2018, **54**, 13837–13840.

6676 | *Inorg. Chem. Front.*, 2024, **11**, 6671–6678

This journal is © the Partner Organisations 2024

15 C. Besnard, C. Svensson, K. Ståhl and T. Siegrist, $Re_4As_6S_3$, a thio-spinel-related cluster system, *J. Solid State Chem.*, 2003, **172**, 446–450.

16 J.-J. Kim, K. Yoon, I. Park and K. Kang, Progress in the development of sodium-ion solid electrolytes, *Small Methods*, 2017, **1**, 1700219.

17 J. Huang, K. Wu, G. Xu, M. Wu, S. Dou and C. Wu, Recent progress and strategic perspectives of inorganic solid electrolytes: Fundamentals, modifications, and applications in sodium metal batteries, *Chem. Soc. Rev.*, 2023, **52**, 4933–4995.

18 X. Feng, H. Fang, N. Wu, P. Liu, P. Jena, J. Nanda and D. Mitlin, Review of modification strategies in emerging inorganic solid-state electrolytes for lithium, sodium, and potassium batteries, *Joule*, 2022, **6**, 543–587.

19 L. Zhang, Y. Liu, J. Han, C. Yang, X. Zhou, Y. Yuan and Y. You, Al doped into Si/P sites of $Na_3Zr_2Si_2PO_{12}$ with conducted Na_3PO_4 impurities for enhanced ionic conductivity, *ACS Appl. Mater. Interfaces*, 2023, **15**, 44867–44875.

20 L. Malatesta, C. Lock and G. Wilkinson, Rhenium(III) iodide, *Inorg. Synth.*, 1963, **7**, 185–189.

21 *APEX2 (version 1.08), SAINT (version 7.03), SADABS (version 2.11)*, Bruker Advanced X-ray Solutions, Madison, WI, USA, 2004.

22 G. Sheldrick, Crystal structure refinement with SHELXL, *Acta Crystallogr., Sect. C: Struct. Chem.*, 2015, **71**, 3–8.

23 *Diamond (version 3.2a)*, Crystal Impact GbR, Bonn, Germany, 2009.

24 P. Vadhva, J. Hu, M. J. Johnson, R. Stocker, M. Braglia, D. J. L. Brett and A. J. E. Rettie, Electrochemical impedance spectroscopy for all-solid-state batteries: Theory, methods and future outlook, *ChemElectroChem*, 2021, **8**, 1930–1947.

25 A. S. Pronin, Y. M. Gayfulin, A. I. Smolentsev and Y. V. Mironov, Tetrahedral rhenium cluster complexes with mixed-ligand cores $\{Re_4As_3Q\}^{5+}$ (Q = S, Se) and $\{Re_4As_2S_2\}^{6+}$, *J. Cluster Sci.*, 2019, **30**, 1253–1257.

26 A. S. Pronin, A. I. Smolentsev, S. G. Kozlova, I. N. Novozhilov and Y. V. Mironov, PO_2^{3-} and AsO^{3-}: Pnictogenide ligands in the highly charged Re_4 cluster anions $[\{Re_4(Po)_3(PO_2)\}(CN)_{12}]^{8-}$, $[\{Re_4As_2(AsO)_2\}(CN)_{12}]^{8-}$, and $[\{Re_4(AsO)_4\}(CN)_{12}]^{8-}$, *Inorg. Chem.*, 2019, **58**, 7368–7373.

27 A. S. Pronin, A. I. Smolentsev and Y. V. Mironov, Inorganic ligands Sb^{3-} and Bi^{3-}: Synthesis and crystal structures of complexes with mixed-ligand cluster cores $\{Re_4Se_3Sb\}^{7+}$ and $\{Re_4Se_3Bi\}^{7+}$, *Inorg. Chem.*, 2021, **60**, 4371–4374.

28 A. S. Pronin, Y. M. Gayfulin, T. S. Sukhikh and Y. V. Mironov, Selective oxidation of inner pnictogenide ligands in mixed-ligand rhenium cubane-type cluster complexes, *Inorg. Chem.*, 2022, **61**, 19756–19763.

29 O. A. Efremova, Y. V. Mironov and V. E. Fedorov, Design of cyano-bridged coordination polymers based on tetrahedral rhenium cluster cyanide complexes and 3d transition metals, *Eur. J. Inorg. Chem.*, 2006, **2006**, 2533–2549.

30 A. Lupan and R. B. King, Hypoelectronic dirhenaboranes having eight to twelve vertices: Internal versus surface rhenium–rhenium bonding, *Inorg. Chem.*, 2012, **51**, 7609–7616.

31 A. Decker, F. Simon, K. Boubekeur, D. Fenske and P. Batail, Neutral and cationic hexanuclear rhenium phosphine clusters with μ_3-(phosphido-chalcogenido), μ_3-(arsenido-chalcogenido), and μ_3-(imido or oxo-chalcogenido) hetero ligand shells, *Z. Anorg. Allg. Chem.*, 2000, **626**, 309–313.

32 T. Kim, S. H. Ahn, Y.-Y. Song, B. J. Park, C. Lee, A. Choi, M.-H. Kim, D.-H. Seo, S.-K. Jung and H.-W. Lee, Prussian blue-type sodium-ion conducting solid electrolytes for all solid-state batteries, *Angew. Chem., Int. Ed.*, 2023, **62**, e202309852.

33 R. Matsuoka, M. Shibata, K. Matsuo, R. Sai, H. Tsutsumi, K. Fujii and Y. Katayama, Importance of lithium coordination structure to lithium-ion transport in polyether electrolytes with cyanoethoxy side chains: An experimental and theoretical approach, *Macromolecules*, 2020, **53**, 9480–9490.

34 X. Cui, F. Tang, Y. Zhang, C. Li, D. Zhao, F. Zhou, S. Li and H. Feng, Influences of trace water on electrochemical performances for lithium hexafluoro phosphate- and lithium bis(oxalato)borate-based electrolytes, *Electrochim. Acta*, 2018, **273**, 191–199.

35 T. Bezrodna, G. Puchkovska, V. Shymanovska, J. Baran and H. Ratajczak, IR-analysis of H-bonded H_2O on the pure TiO_2 surface, *J. Mol. Struct.*, 2004, **700**, 175–181.

36 Z. Deng, T. P. Mishra, E. Mahayoni, Q. Ma, A. J. K. Tieu, O. Guillon, J.-N. Chotard, V. Seznec, A. K. Cheetham, C. Masquelier, G. S. Gautam and P. Canepa, Fundamental investigations on the sodium-ion transport properties of mixed polyanion solid-state battery electrolytes, *Nat. Commun.*, 2022, **13**, 4470.

37 A. E. Maughan, Y. Ha, R. T. Pekarek and M. C. Schulze, Lowering the activation barriers for lithium-ion conductivity through orientational disorder in the cyanide argyrodite Li_6PS_5CN, *Chem. Mater.*, 2021, **33**, 5127–5136.

38 M. Joos, M. Conrad, A. Rad, P. Kaghazchi, S. Bette, R. Merkle, R. E. Dinnebier, T. Schleid and J. Maier, Ion transport mechanism in anhydrous lithium thiocyanate liscn part i: Ionic conductivity and defect chemistry, *Phys. Chem. Chem. Phys.*, 2022, **24**, 20189–20197.

39 P. Raizada, V. Soni, A. Kumar, P. Singh, A. A. P. Khan, A. M. Asiri, V. K. Thakur and V.-H. Nguyen, Surface defect engineering of metal oxides photocatalyst for energy application and water treatment, *J. Materiomics*, 2021, **7**, 388–418.

40 Y. Xiao, Y. Wang, S.-H. Bo, J. C. Kim, L. J. Miara and G. Ceder, Understanding interface stability in solid-state batteries, *Nat. Rev. Mater.*, 2020, **5**, 105–126.

41 Q. Shi, Y. Zhong, M. Wu, H. Wang and H. Wang, High-performance sodium metal anodes enabled by a bifunctional potassium salt, *Angew. Chem., Int. Ed.*, 2018, **57**, 9069–9072.

42 M. Yang, X. Chang, L. Wang, X. Wang, M. Gu, H. Huang, L. Tang, Y. Zhong and H. Xia, Interface modulation of metal sulfide anodes for long-cycle-life sodium-ion batteries, *Adv. Mater.*, 2023, **35**, 2208705.

This journal is © the Partner Organisations 2024

Inorg. Chem. Front., 2024, **11**, 6671–6678 | **6677**

43 R. Damircheli, B. Hoang, V. C. Ferrari and C.-F. Lin, Fluorinated artificial solid–electrolyte–interphase layer for long-life sodium metal batteries, *ACS Appl. Mater. Interfaces*, 2023, **15**, 54915–54922.

44 C. Wang, Z. Sun, L. Liu, H. Ni, Q. Hou, J. Fan, R. Yuan, M. Zheng and Q. Dong, A rooted interphase on sodium via in situ pre-implantation of fluorine atoms for high-performance sodium metal batteries, *Energy Environ. Sci.*, 2023, **16**, 3098–3109.